Article

Pulsed EPR Investigations of Systems Modeling Molybdenum Enzymes: Hyperfine and Quadrupole Parameters of Oxo-O in [MoO(SPh)]

Andrei V. Astashkin, Frank Neese, Arnold M. Raitsimring,
J. Jon A. Cooney, Eric Bultman, and John H. Enemark

J. Am. Chem. Soc., **2005**, 127 (47), 16713-16722• DOI: 10.1021/ja055472y • Publication Date (Web): 05 November 2005

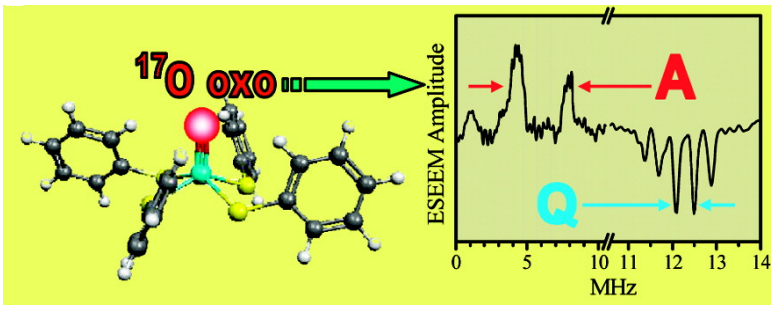

More About This Article

Additional resources and features associated with this article are available within the HTML version:

- Supporting Information
- Links to the 8 articles that cite this article, as of the time of this article download
- Access to high resolution figures
- Links to articles and content related to this article
- Copyright permission to reproduce figures and/or text from this article

View the Full Text HTML

J|A|C|S
ARTICLES
Published on Web 11/05/2005

Pulsed EPR Investigations of Systems Modeling Molybdenum Enzymes: Hyperfine and Quadrupole Parameters of Oxo-^{17}O in $[Mo^{17}O(SPh)_4]^-$

Andrei V. Astashkin,*,† Frank Neese,*,‡ Arnold M. Raitsimring,*,† J. Jon A. Cooney,† Eric Bultman,†,§ and John H. Enemark*,†

Contribution from the Department of Chemistry, University of Arizona, Tucson, Arizona 85721, and Max-Planck Institut für Bioanorganische Chemie, Stiftstrasse, 34-36, 45470 Mülheim an der Ruhr, Germany

Received August 10, 2005; E-mail: arnold@u.arizona.edu

Abstract: K_a band ESEEM spectroscopy was used to determine the hyperfine (*hfi*) and nuclear quadrupole (*nqi*) interaction parameters for the oxo-^{17}O ligand in $[Mo^{17}O(SPh)_4]^-$, a spectroscopic model of the oxo-Mo(V) centers of enzymes. The isotropic *hfi* constant of 6.5 MHz found for the oxo-^{17}O is much smaller than the values of ~20−40 MHz typical for the ^{17}O nucleus of an equatorial $OH_{(2)}$ ligand in molybdenum enzymes. The ^{17}O *nqi* parameter ($e^2qQ/h = 1.45$ MHz, $\eta \approx 0$) is the first to be obtained for an oxo group in a metal complex. The parameters of the oxo-^{17}O ligand, as well as other magnetic resonance parameters of $[Mo^{17}O(SPh)_4]^-$ predicted by quasi-relativistic DFT calculations, were in good agreement with those obtained in experiment. From the electronic structure of the complex revealed by DFT, it follows that the SOMO is almost entirely molybdenum d_{xy} and sulfur p, while the spin density on the oxo-^{17}O is negative, determined by spin polarization mechanisms. The results of this work will enable direct experimental identification of the oxo ligand in a variety of chemical and biological systems.

Introduction

Electron paramagnetic resonance (EPR) has long been a convenient and direct probe of the active sites of molybdoenzymes, such as sulfite oxidase (SO), xanthine oxidase (XO), and dimethyl sulfoxide (DMSO) reductase. Structural interpretation of EPR data from the enzymes has been greatly aided by comparison with the EPR data from a wide range of synthetic molybdenum(V) complexes of known structure. These synthetic complexes include $Mo(abt)_3$ ($abtH_2$ = *o*-aminobenzenethiol), $[MoO(XPh)_4]^-$ (X = S, Se), *cis*-$[MoO(qtl)_2X]$ (X = Cl, Br; qtlH = quinoline-8-thiol),[1−6] $[MoOXL]^-$ and $[MoO(XH)L]$ (X = O, S; LH_2 = *N*,*N*′-bis(2-mercaptophenyl)-1,2-diaminoethane),[7−9] and (Tp*)$MoOX_2$ (Tp* = hydrotris(3,5-dimethyl-1-pyrazolyl)borate, X = Cl, NCS, N_3, SR, OR).[10] Although the EPR experiments were mostly continuous wave (CW), the use of isotopic substitutions and multifrequency EPR led to dramatic improvements in the quantity and quality of the data related to the ligand hyperfine interactions (*hfi*) in Mo(V) complexes.[6] In particular, these studies of model compounds provided very useful correlations between the *g* values, the nature of atoms directly coordinated to Mo(V), and the amount of spin population transferred from Mo(V) to the ligands. Specifically, for oxygen ligands, it was shown that the *hfi* of an axial oxo-^{17}O is substantially weaker than that of a water or hydroxyl oxygen coordinated in the equatorial plane.[8,9] This result allowed assignment of the oxygen ligands in xanthine oxidase, which provided a deep insight into structure and function of this enzyme.[11]

Our current interest in model Mo(V) complexes is stimulated by the results of our recent investigation of the Mo(V) center of the high-pH (*hpH*) form of SO in ^{17}O-enriched water using electron spin−echo envelope modulation (ESEEM) spectroscopy in the microwave (mw) K_a band.[12] That study revealed the presence of a weakly magnetically coupled ^{17}O ligand, in addition to a strongly magnetically coupled ^{17}O from the equatorial water/hydroxyl ligand that was detected previously

† University of Arizona.
‡ Max-Planck Institut für Bioanorganische Chemie.
§ Beckman Scholar.

(1) Hanson, G. R.; Brunette, A. A.; McDonell, A. C.; Murray, K. S.; Wedd, A. G. *J. Am. Chem. Soc.* **1981**, *103*, 1953−1959.
(2) Boyd, I. W.; Dance, I. G.; Murray, K. S.; Wedd, A. G. *Aust. J. Chem.* **1978**, *31*, 279−284.
(3) Dance, I. G.; Wedd, A. G.; Boyd, I. W. *Aust. J. Chem.* **1978**, *31*, 519−526.
(4) Bradbury, J. R.; Mackay, M. F.; Wedd, A. G. *Aust. J. Chem.* **1978**, *31*, 2423−2430.
(5) Cramer, S. P.; Johnson, J. L.; Rajagopalan, K. V.; Sorrell, T. N. *Biochem. Biophys. Res. Commun.* **1979**, *91*, 434−439.
(6) Hanson, G. R.; Wilson, G. L.; Bailey, T. D.; Pilbrow, J. R.; Wedd, A. G. *J. Am. Chem. Soc.* **1987**, *109*, 2609−2616.
(7) Farchione, F.; Hanson, G. R.; Rodrigues, C. G.; Bailey, T. D.; Bagchi, R. N.; Bond, A. M.; Pilbrow, J. R.; Wedd, A. G. *J. Am. Chem. Soc.* **1986**, *108*, 831−832.
(8) Dowerah, D.; Spence, J. T.; Singh, R.; Wedd, A. G.; Wilson, G. L.; Farchione, F.; Enemark, J. H.; Kristofzski, J. G.; Bruck, M. A. *J. Am. Chem. Soc.* **1987**, *109*, 5655−5665.
(9) Wilson, G. L.; Kony, M.; Tiekink, E. R. T.; Pilbrow, J. R.; Spence, J. T.; Wedd, A. G. *J. Am. Chem. Soc.* **1988**, *110*, 6923−6925.
(10) Cleland, W. E., Jr.; Barnhart, K. M.; Yamanouchi, K.; Collison, D.; Mabbs, F. E.; Ortega, R. B.; Enemark, J. H. *Inorg. Chem.* **1987**, *26*, 1017−1025.
(11) Greenwood, R. J.; Wilson, G. L.; Pilbrow, J. R.; Wedd, A. G. *J. Am. Chem. Soc.* **1993**, *115*, 5385−5392.
(12) Astashkin, A. V.; Feng, C.; Raitsimring, A. M.; Enemark, J. H. *J. Am. Chem. Soc.* **2005**, *127*, 502−503.

by CW EPR.[13] The *hfi* parameters of this weakly coupled ^{17}O ligand were similar to those estimated earlier by CW EPR for the model oxomolybdenum(V) complex, $[Mo^{17}O(SPh)_4]^-$,[1,5,6] which led us to tentatively assign this ligand in SO as an axial oxo-^{17}O. An alternative option that could not be completely ruled out was to assign this oxygen to an axial ^{17}OH ligand.[12] To conclusively decide in favor of one of these options, further investigation of SO as well as of model systems is necessary. In particular, it is desirable to obtain information about the nuclear quadrupole interaction (*nqi*) tensor of an oxo-^{17}O in a model system, which is a valuable parameter for distinguishing between different kinds of oxygen ligands. Quite understandably, no *nqi* data for the oxo-^{17}O were obtained by CW EPR,[1,5,6] and to our knowledge, no such data are currently available in the literature.

Therefore, in this work, we undertook a ^{17}O ESEEM study of the model oxomolybdenum complex, $[Mo^{17}O(SPh)_4]^-$. The purposes of this investigation were to obtain the *nqi* parameters for the oxo-^{17}O ligand and to improve the accuracy of the *hfi* parameters. The *hfi* and *nqi* parameters obtained were analyzed in terms of the electronic structure, both qualitatively and using density functional theory (DFT) calculations. The success of DFT in reproducing the characteristic values of the *hfi* and *nqi* parameters for the oxo-^{17}O allows one to expect a similar degree of success in the applications of DFT to SO and other molybdoenzymes.

Materials and Methods

Synthesis of $[Mo^{17}O(SPh)_4]^-$. $[PPh_4][Mo^{17}OCl_4]$ was prepared by a method analogous to that for $[PPh_4][MoOCl_4]$.[14] Water (50 μL of 70 mol % of $H_2{}^{17}O$, an excess) was added to a red/brown mixture of $MoCl_5$ (0.06 g) and dry PPh_4Cl (0.082 g, dried under vacuum for 48 h) in DCM (8 cm^3) and stirred vigorously for 3 min. The resulting pale green solution was filtered, carefully layered with hexane (8 cm^3), and allowed to stand for 48 h to yield green crystals of $[PPh_4][Mo^{17}OCl_4]$.

$[Mo^{17}O(SPh)_4]^-$ was prepared by the method of Hanson et al.[1] A solution of MeCN (20 cm^3), DMF (5 cm^3), NEt_3 (0.7 cm^3), and HSPh (0.027 g) was prepared. A 4.3 cm^3 aliquot was then added to 0.05 g of $[PPh_4][Mo^{17}OCl_4]$. The resultant solution was filtered directly into the EPR tubes. The majority of the counterion was presumed to be $[NEt_3H]^+$.

Pulsed EPR Measurements. ESEEM measurements were performed on a home-built K_a band pulsed EPR spectrometer[15] that operates in the mw frequency range from 26.5 to 40 GHz. The specific mw frequency of 29.372 GHz and the range of magnetic fields from 1030 to 1060 mT used in our experiments provided the so-called "weak interaction" conditions, in which the *hfi* constant of ^{17}O ($a_{iso} \approx 6.6$ MHz[1]) was less than twice its Zeeman frequency. This facilitated a simple interpretation of the ESEEM spectra. At the same time, under these experimental conditions, the ^{17}O parameters were not very far into the weak interaction limit, which resulted in an easily measurable ESEEM amplitude.

In our experiments, we used two-pulse (primary) and four-pulse ESEEM techniques. The durations of the 90 and 180° mw pulses were 14 and 25 ns, respectively. These pulses provided a mw field amplitude of about 20 MHz, more than twice as great as the largest frequency of a $\Delta m_I = 1$ transition of ^{17}O. As a result, a nearly complete excitation[16] of the ESEEM harmonics with frequencies up to those corresponding to $\Delta m_I = 2$ transitions of ^{17}O was achieved (which practically represented all easily observable harmonics), and the numerical simulations could be performed in the complete excitation limit. At the same time, the mw amplitude of 20 MHz (which translates to ~0.7 mT excitation width in the EPR spectrum) was only about half of the intrinsic EPR line width and did not significantly affect the orientational selectivity in our measurements. The temperature of measurements was about 20 K.

Density Functional Calculations. All calculations were done with the ORCA package.[17] Two sets of scalar relativistic DFT calculations were carried out. The first set of calculations was done on the experimental structure.[4] The second set was performed on geometry optimized structures. Optimizations were done in redundant internal coordinates using the built-in optimizer of ORCA and using the BP86 functional,[18,19] the SV(P) (on H and C),[20] and TZVP (on Mo and S)[21,22] basis sets, the RI approximation,[23,24] and the COSMO solvent model[25] (with $\epsilon = 80$ simulating a polar environment) together with the ZORA-(MP)[26,27] scalar relativistic correction in the one-center approximation.[28] The coordinates for the optimized structure are given in Table S1.

Property calculations were done at the two above-mentioned geometries and the B3LYP and BP86 functionals. Again, the COSMO-(water) solvation model was employed together with the scalar relativistic ZORA(MP) method (but without the one-center approximation). The property calculations used an extensive uncontracted basis set at the Mo center (28*s*20*p*17*d*),[29,30] the uncontracted TZVP basis on sulfur (14*s*9*p*1*d*), and the uncontracted IGLO-III basis[31] on oxygen (11*s*7*p*2*d*). The carbons were described with the uncontracted SVP basis (7*s*4*p*1*d*), while the hydrogens were described with the uncontracted SV basis (4*s*). Altogether, this calculation used 1055 basis functions.

The g-tensors were calculated according to the coupled-perturbed Kohn−Sham procedure as described previously.[32] A-tensors were evaluated according to the procedure of van Lenthe in the ZORA formalism.[33] Spin−orbit coupling contributions were treated with the coupled-perturbed Kohn−Sham method outlined previously.[34] SOC corrections for both Mo and O were computed. For the field gradient, we used the straight ZORA electron density since we have found in a recent study that the ZORA-4 formalism does not improve the results of ZORA calculations relative to four-component reference calculations.[35] The SOC operator was the accurate SOMF approximation[36] in

(13) Cramer, S. P.; Johnson, J. L.; Rajagopalan, K. V.; Sorrell, T. N. *Biochem. Biophys. Res. Commun.* **1979**, *91*, 434−439.
(14) Carducci, M. D. Ph.D. Dissertation, University of Arizona, 1994, 335.
(15) Enemark, J. H.; Raitsimring, A. M.; Astashkin, A. V.; Walker, F. A. *K_a-Band (27−40 GHz) Pulsed EPR Spectrometer of the University of Arizona;* 46th Rocky Mountain Conference on Analytical Chemistry; American Chemical Society: Washington, DC, 2004; Vol. 46.
(16) Dikanov, S. A.; Tsvetkov, Y. D. In *Electron Spin−Echo Envelope Modulation (ESEEM) Spectroscopy;* CRC Press: Boca Raton, FL, 1992.
(17) Neese, F. *ORCA: An ab initio, Density Functional and Semiempirical Program Package*, version 2.4, revision 24, August 2004.
(18) Becke, A. D. *Phys. Rev. A: At. Mol. Opt. Phys* **1988**, *38*, 3098−3100.
(19) Perdew, J. P. *Phys. Rev. B* **1986**, *33*, 8822−8824.
(20) Schäfer, A.; Horn, H.; Ahlrichs, R. *J. Chem. Phys.* **1992**, *97*, 2571−2577.
(21) Schäfer, A.; Huber, C.; Ahlrichs, R. *J. Chem. Phys.* **1994**, *100*, 5829−5835.
(22) Ahlrichs, R.; May, K. *Phys. Chem. Chem. Phys.* **2000**, *2*, 943−945.
(23) Eichkorn, K.; Weigend, F.; Treutler, O.; Ahlrichs, R. *Theor. Chem. Acc.* **1997**, *97*, 119−124.
(24) Eichkorn, K.; Treutler, O.; Öhm, H.; Häser, M.; Ahlrichs, R. *Chem. Phys. Lett.* **1995**, *240*, 283−290.
(25) Klamt, A.; Schüürmann, G. *J. Chem. Soc., Perkin Trans. 2* **1993**, 799−805.
(26) van Lenthe, E.; Snijders, J. G.; Baerends, E. J. *J. Chem. Phys.* **1996**, *105*, 6505−6516.
(27) van Wüllen, C. *J. Chem. Phys.* **1998**, *109*, 392−399.
(28) van Lenthe, J. H.; Faas, S.; Snijders, J. G. *Chem. Phys. Lett.* **2000**, *328*, 107−112.
(29) Huzinaga, S.; Miguel, B. *Chem. Phys. Lett.* **1990**, *175*, 289−291.
(30) Huzinaga, S.; Klobukowski, M. *Chem. Phys. Lett.* **1993**, *212*, 260−264.
(31) Kutzelnigg, W.; Fleischer, U.; Schindler, M. In *The IGLO-Method: Ab Initio Calculation and Interpretation of NMR Chemical Shifts and Magnetic Susceptibilities;* Springer-Verlag: Heidelberg, 1990; Vol. 23.
(32) Neese, F. *J. Chem. Phys.* **2001**, *115*, 11080−11096.
(33) van Lenthe, E.; van der Avoird, A.; Wormer, P. E. S. *J. Chem. Phys.* **1998**, *108*, 4783−4796.
(34) Neese, F. *J. Chem. Phys.* **2003**, *118*, 3939−3948.
(35) Neese, F.; Wolf, A.; Fleig, T.; Reiher, M.; Hess, B. A. *J. Chem. Phys.* **2005**, *122*, 204107.
(36) Hess, B. A.; Marian, C. M.; Wahlgren, U.; Gropen, O. *Chem. Phys. Lett.* **1996**, *251*, 365−371.

the multicenter implementation described previously.[37] The auxiliary basis set used in the BP86 calculations as well as for the calculation of the SOC integrals was generated automatically from the orbital basis. Accurate numerical integration in the presence of steep basis functions was ensured by using very dense integration meshes in the core region of the heavy atoms.

ESEEM Theory for ^{17}O

The ^{17}O nucleus has spin $I = 5/2$ and a nonzero quadrupole moment. While there is a considerable body of work, both experimental and theoretical, concerning ESEEM of high-spin ($I > 1/2$) nuclei,[16] most of those studies deal with ^{14}N and ^{2}D (both $I = 1$). The ESEEM investigations of nuclei with $I = 5/2$ (^{17}O, ^{27}Al) are much fewer in number,[38−41] but they provide a sufficient background for understanding the ^{17}O ESEEM observed in this work. The purpose of this section is to introduce the necessary spectroscopic parameters and to show their approximate relation to the ^{17}O frequencies in the ESEEM spectra of the $[Mo^{17}O(SPh)_4]^-$ complex.

The spin Hamiltonian accounting for the nuclear Zeeman interaction, *hfi*, and *nqi* can be written as follows:

$$\hat{H} = -\nu_I \hat{I}_Z + m_S[T_{ZX}\hat{I}_X + T_{ZY}\hat{I}_Y + (a_{iso} + T_{ZZ})\hat{I}_Z] + k[3\hat{I}^2_{Z'} + \eta(\hat{I}^2_{X'} - \hat{I}^2_{Y'})] \quad (1)$$

where ν_I is the Zeeman frequency, a_{iso} is the isotropic *hfi* constant, T_{Zj} (j = X, Y, Z) are the relevant components of the anisotropic *hfi*, k is the nuclear quadrupole coupling constant ($k = e^2Qq/[4I(2I-1)h]$), and η is the asymmetry parameter of the electric field gradient on the nucleus. X, Y, and Z are the axes of the laboratory coordinate frame, with $\mathbf{B}_o$ // Z. X′, Y′, and Z′ are the principal axes of the *nqi*. The electron spin projection on $\mathbf{B}_o$, m_S ($m_S \equiv \langle S_Z \rangle$), assumes the values of $-1/2$ and $1/2$.

Let us consider first the ESEEM frequencies. To obtain approximate expressions necessary for a qualitative analysis, we will omit the nonsecular part of the Hamiltonian eq 1:

$$\hat{H} = -\nu_I \hat{I}_Z + m_S(a_{iso} + T_{ZZ})\hat{I}_Z + \tilde{Q}\hat{I}_Z{}^2 \quad (2)$$

where $\tilde{Q} = 3/2k[3b^2_{Z'Z} - 1 + \eta(b^2_{X'Z} - b^2_{Y'Z})]$, and $b_{X'Z}$, $b_{Y'Z}$, and $b_{Z'Z}$ are the direction cosines of the Z axis in the X′Y′Z′ frame. We will denote the transition frequencies between the nuclear spin projections m_I and $m_I + \Delta m_I$ ($m_I \equiv \langle I_Z \rangle$) within the α and β electron spin manifolds as $\nu_\alpha^{\Delta m_I}$ and $\nu_\beta^{\Delta m_I}$. These frequencies are given by

$$\nu_{\alpha,\beta}{}^{\Delta m_I} = \left[-\nu_I \pm \frac{1}{2}(a_{iso} + T_{ZZ}) + \tilde{Q}(2m_I + \Delta m_I)\right]\cdot \Delta m_I \quad (3)$$

In particular, for the $\Delta m_I = 1$ transition, one obtains

$$\nu^1_{\alpha,\beta} = -\nu_I \pm \frac{1}{2}(a_{iso} + T_{ZZ}) + \tilde{Q}(2m_I + 1) \quad (4)$$

In the case of weak *nqi*, obviously, $\nu_{\alpha,\beta}^{\Delta m_I} \approx \Delta m_I \cdot \nu^1_{\alpha,\beta}$.

From eq 3, one can see that each of the fundamental frequencies, collectively denoted $\nu_\alpha^{\Delta m_I}$ and $\nu_\beta^{\Delta m_I}$, actually splits into $2I + 1 - \Delta m_I$ different frequencies that depend on the specific m_I values involved in the nuclear transition. The splitting between the spectral lines $\nu_{\alpha,\beta}^{\Delta m_I}$ corresponding to the nuclear transitions $m_I \leftrightarrow m_I + \Delta m_I$ (denoted $\nu_{\alpha,\beta}^{\Delta m_I}(m_I)$) and $m_I + 1 \leftrightarrow m_I + 1 + \Delta m_I$ (denoted $\nu_{\alpha,\beta}^{\Delta m_I}(m_I + 1)$), as obtained from eq 3, is equal to

$$\Delta\nu_{\alpha,\beta}^{\Delta m_I} = |\nu_{\alpha,\beta}^{\Delta m_I}(m_I + 1) - \nu_{\alpha,\beta}^{\Delta m_I}(m_I)| = 2|\tilde{Q}\Delta m_I| \quad (5)$$

In this approximation, the splitting is purely due to the *nqi*. In most cases, however, it cannot be used to experimentally determine the *nqi* parameters because the *hfi* distribution, whether purely statistical or because of the *hfi* anisotropy, will broaden the individual $\nu_{\alpha,\beta}^{\Delta m_I}(m_I)$ lines to the extent that small quadrupolar splittings cannot be resolved.

Along with fundamental frequencies given by eqs 3 and 4, in many ESEEM techniques, combination frequencies are also observed. Thus, for a system with $I = 1/2$, one can observe the sum and difference combinations of ν^1_α and ν^1_β, $\nu^1_\sigma = \nu^1_\alpha + \nu^1_\beta$ and $\nu_\delta{}^1 = |\nu^1_\alpha - \nu^1_\beta|$, respectively. For $I > 1/2$, however, all other possible combinations of fundamental frequencies in α and β manifolds (e.g., $\nu^2_\alpha + \nu^1_\beta$ or $|\nu^2_\alpha - \nu^1_\beta|$) may also contribute to the ESEEM spectra. From a practical standpoint, the sum combination frequency $\nu^1_\sigma = \nu^1_\alpha + \nu^1_\beta$ is the most interesting one because in favorable conditions it may allow one to easily estimate the *nqi* parameters. The idea, first investigated theoretically elsewhere,[38−41] follows from the explicit expression for ν^1_σ:

$$\nu^1_\sigma(m_I) = \nu^1_\alpha(m_I) + \nu^1_\beta(m_I) = -2\nu_I + 2\tilde{Q}(2m_I + 1) \quad (6)$$

As with the fundamental frequency discussed above, the generic sum combination frequency ν^1_σ splits into a quintet of frequencies corresponding to different transitions $m_I \leftrightarrow m_I + 1$. The splitting between the frequencies in this sum combination quintet is obviously

$$\Delta\nu^1_\sigma = |\nu^1_\sigma(m_I + 1) - \nu^1_\sigma(m_I)| = 4|\tilde{Q}| \quad (7)$$

The splitting is again due to the *nqi* only. In this case, however, the individual $\nu^1_\sigma(m_I)$ lines in an ESEEM spectrum are not broadened by the *hfi* distribution (see eq 6), and in favorable cases, the splitting of the sum combination line ν^1_σ into a quintet can be observed.

Our discussion so far was based on the simplified Hamiltonian given by eq 2 that did not contain any nonsecular terms. Neglecting these terms is reasonable for a qualitative discussion if the anisotropic hyperfine (T_{ij}) and quadrupolar (k) coupling constants (in frequency units) are small compared with the nuclear transition frequencies. The analysis of the experimental data in the following sections shows that this represents a good approximation for the oxo-^{17}O ligand in $[MoO(SPh)_4]^-$, when the experiments are performed in the mw K_a band.

The accuracy of the expressions for the ESEEM frequencies would be improved by including the nonsecular terms, but at the expense of making the equations less transparent and less suitable for a qualitative discussion. More importantly, it is due to the nonsecular terms that the nuclear eigenstates within one of the electron spin manifolds become generally nonorthogonal to more than one eigenstate within the other manifold, which is a necessary condition for the ESEEM to appear at all. As a

(37) Neese, F. *J. Chem. Phys.* **2005**, *122*, 034107/1−034107/13.
(38) Thomann, H.; Bernardo, M.; Goldfarb, D.; Kroneck, P. M. H.; Ullrich, V. *J. Am. Chem. Soc.* **1995**, *117*, 8243−8251.
(39) Matar, K.; Goldfarb, D. *J. Magn. Reson., Ser. A* **1994**, *111*, 50−61.
(40) Matar, K.; Goldfarb, D. *J. Chem. Phys.* **1992**, *96*, 6464−6476.
(41) Matar, K.; Goldfarb, D. *J. Phys. Chem.* **1992**, *96*, 3100−3109.

simple demonstration of how the nonsecular terms of Hamiltonian 1 determine the ESEEM amplitude for $I = 5/2$, one can use the following expression for the primary ESEEM derived from a general formula for the case of arbitrary spin and zero *nqi*:[42]

$$V_{5/2}(\tau) = \frac{1}{3}[16V^5_{1/2}(\tau) - 16V^3_{1/2}(\tau) + 3V_{1/2}(\tau)] \qquad (8)$$

where

$$V_{1/2}(\tau) = \left[1 - \frac{k_m}{2}\left(1 - \cos\omega^1_\alpha\tau - \cos\omega^1_\beta\tau + \frac{1}{2}\cos\omega^1_\sigma\tau + \frac{1}{2}\cos\omega^1_\delta\tau\right)\right] \qquad (9)$$

is the primary ESEEM for $I = 1/2$, τ is the time interval between the mw pulses, and $\omega^1_{\alpha,\beta,\sigma,\delta} = 2\pi\nu^1_{\alpha,\beta,\sigma,\delta}$. The ESEEM amplitude factor is given by[43]

$$k_m = \frac{\nu_I^2(T^2_{ZX} + T^2_{ZY})}{\nu^2_\alpha\,\nu^2_\beta} \qquad (10)$$

In this *hfi*-only approximation, the ESEEM amplitude is determined by the nonsecular terms related to the anisotropic *hfi*. For weak *nqi*, however, it is still a very good approximation because the weak *nqi* primarily affects the ESEEM frequencies.[16]

From eq 8, it follows that the fundamental harmonics $\nu^{\Delta m_I}_{\alpha,\beta}$ (in the case of zero *nqi* $\nu^{\Delta m_I}_{\alpha,\beta} = \Delta m_I \cdot \nu^1_{\alpha,\beta}$; see above) will have relative amplitudes $\propto k^{\Delta m_I}_m$. If the anisotropic *hfi* is sufficiently weak, then $k_m \ll 1$, and the amplitude of these harmonics will rapidly decrease with increasing Δm_I. Therefore, in the limit of weak *hfi* and *nqi*, the fundamental lines of $\Delta m_I = 1$ transitions in ESEEM spectra will have the largest amplitude among all fundamental lines.

The features of the ESEEM spectra for $I = 5/2$ described here will facilitate the qualitative understanding of the experimental spectra of $[Mo^{17}O(SPh)_4]^-$. The expressions given in this section will also provide preliminary estimates for the *hfi* and *nqi* parameters of the oxo-^{17}O ligand. The refinement of these parameters, however, will be done using ESEEM simulations based on numerical diagonalization of the full spin-Hamiltonian (eq 1) and the density matrix formalism.

Results and Discussion

Field-Sweep Spectrum. The field-sweep spectrum of $[Mo^{17}O(SPh)_4]^-$ detected using the primary ESE technique is shown in Figure 1. As expected from the C_4 symmetry of the complex, and in agreement with results reported elsewhere,[1] the g-tensor is essentially axial, with $g_\parallel \approx 2.019$ and $g_\perp \approx 1.982$. A small shoulder at the high-field side of the spectrum is due to the ^{95}Mo isotope.[1] The spectrum of the complex with natural abundance of ^{17}O (i.e., essentially, $[Mo^{16}O(SPh)_4]^-$) was identical. Since the spectrum in Figure 1 does not exhibit any features attributable to ^{17}O, ESEEM experiments have been performed in order to determine the spectroscopic parameters of the oxo-^{17}O ligand. Although several ESEEM techniques have been tried, the most productive ones were the primary ESEEM, which allowed us to easily determine the *hfi* tensor, and the integrated four-pulse ESEEM that allowed us to determine the *nqi* tensor. Below, we consider the ESEEM results in detail.

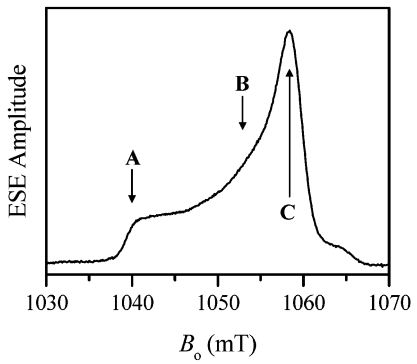

Figure 1. Field-sweep spectrum of $[Mo^{17}O(SPh)_4]^-$ recorded using a two-pulse ESE technique. Experimental conditions: mw frequency = 29.372 GHz; mw pulses = 2 × 17 ns; time interval between the mw pulses = τ = 200 ns. Points A ($\mathbf{B}_o$ = 1040 mT), B ($\mathbf{B}_o$ = 1053 mT), and C ($\mathbf{B}_o$ = 1058.3 mT) correspond to the angles between the $g_\parallel$ axis and $\mathbf{B}_o$ of 11, 56, and 79°, respectively.

For convenience, we will use in the following the molecular coordinate frame (*x*, *y*, *z*) with the *z*-axis being parallel to the Mo≡O bond, and with the *x*- and *y*-axes being parallel to two mutually perpendicular O−Mo−S planes. The ESEEM measurements were performed at several positions in the EPR spectrum that corresponded to different angles θ between the external magnetic field $\mathbf{B}_o$ and the $g_\parallel$ axis. By symmetry, the $g_\parallel$ axis is parallel to the Mo≡O bond and, by definition, to the *z*-axis. For a position within the EPR spectrum that corresponds to a g-factor of *g*, the angle θ is found from

$$\cos^2\theta = \frac{g^2 - g^2_\perp}{g^2_\parallel - g^2_\perp} \qquad (11)$$

The *hfi* and *nqi* tensors obtained from the ESEEM analysis described below were axial, with the main axes being parallel to *z*. Therefore, although the measurements were performed at many EPR positions, we only present the spectra obtained at EPR positions A (near $g_\parallel$, $\theta \approx 11°$), B ($\theta \approx 56°$, close to the magic angle), and C (near $g_\perp$, $\theta \approx 79°$) marked in Figure 1.

Primary ESEEM Spectra. Determination of *hfi* Parameters. The primary ESEEM spectra obtained at EPR positions A and C for $[Mo^{17}O(SPh)_4]^-$ and $[Mo^{16}O(SPh)_4]^-$ are shown in the Supporting Information (Figure S1). One of the lines observed in these spectra is easily recognizable; it is a weak line with positive amplitude at the proton Zeeman frequency, $\nu_H \sim 45$ MHz. This line is caused by the *hfi* of the unpaired electron of Mo(V) with numerous protons of the solvent and ligands. In addition to the ν_H line, there are multiple lines in the low-frequency region that are only observed for the sample with ^{17}O (compare solid and dashed traces in Figure S1). The latter fact indicates that these are the lines of ^{17}O nuclear transitions (with positive amplitude) and their linear combinations (with negative amplitude).

Figure 2 shows the low-frequency part of the primary ESEEM spectra obtained at EPR positions A, B, and C. In each spectrum, one can see a pair of prominent lines with positive amplitude, situated symmetrically with respect to the ^{17}O Zeeman frequency, ν_O, that varies from 6.0 MHz (trace A) to 6.1 MHz

(42) Dikanov, S. A.; Shubin, A. A.; Parmon, V. N. *J. Magn. Reson.* **1981**, *42*, 474−487.
(43) Mims, W. B. *Phys. Rev. B: Solid State* **1972**, *3*, 2409−2419.

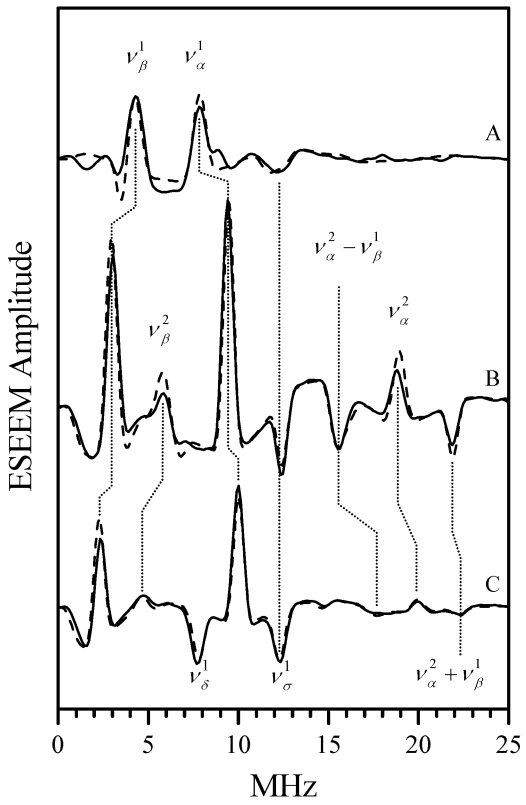

Figure 2. Solid traces A, B, and C, cosine Fourier transforms (low-frequency part) of the primary ESEEM of $[Mo^{17}O(SPh)_4]^-$ obtained at EPR positions A, B, and C, respectively (see Figure 1). Experimental conditions: mw frequency = 29.372 GHz; mw pulses = 2 × 17 ns; dead time = τ_d = 120 ns. Dashed traces show the corresponding simulated primary ESEEM spectra. The simulation parameters were as follows: nucleus, ^{17}O; isotropic *hfi* constant, a_{iso} = 6.5 MHz; anisotropic *hfi* tensor was axial, with $T_\perp$ = 1.6 MHz; *nqi* tensor was axial, with the quadrupole coupling constant e^2Qq/h = 1.45 MHz. The axes of the *hfi*, *nqi*, and g-tensors were coincident. The assignments of the clearly visible lines are indicated.

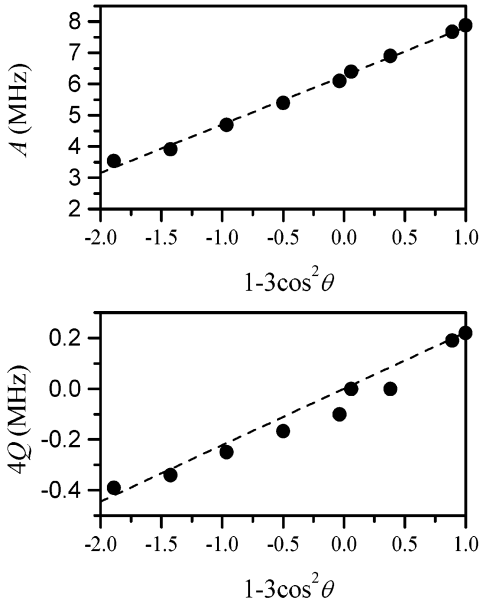

Figure 3. The dependences of the hyperfine (a) and quadrupole (b) splittings on $1 - 3\cos^2\theta$, where θ is the angle between the $g_{||}$ axis and $\mathbf{B}_o$. The hyperfine splitting was determined as the splitting between the lines ν^1_α and ν^1_β in the primary ESEEM spectra (see Figure 2). The quadrupole splitting was determined as the splitting between the adjacent component lines of the ν^1_σ quintet (see Figure 4 and eq 7). Dashed lines represent least-squares fits.

(trace C). Based on the discussion in the Theory section, these lines can be attributed to the $\Delta m_I = 1$ transition frequencies ν^1_α and ν^1_β. Although it is not possible to say which of these lines corresponds to the α electron spin manifold and which to the β manifold, we have tentatively assigned the high-frequency line to the α-manifold. The opposite assignment will ultimately result in the simultaneous change of the sign of all *hfi* parameters.

The line with negative amplitude at the frequency of about 12 MHz is a sum combination line ν^1_σ. The positive line at the frequency of ~19.5 MHz in spectrum B is the fundamental line of the $\Delta m_I = 2$ transitions, ν^2_α. The assignments of all the mentioned lines, as well of other clearly visible lines, are indicated in Figure 2.

The fact that the ν^1_σ line is reasonably narrow (although it broadens somewhat in spectrum A) and does not show any *nqi*-related features indicates that the *nqi* is weak, and the qualitative analysis outlined in the Theory section is applicable. It follows from eq 4 that the centers of gravity of the composite $\nu^1_{\alpha,\beta}$ lines do not depend on *nqi* (to first order in *nqi*) and are approximately located at the frequencies of

$$\langle \nu^1_{\alpha,\beta}(m_I)\rangle_{m_I} = -\nu_O \pm \frac{1}{2}(a_{iso} + T_{ZZ}) \qquad (12)$$

The splitting between these lines then gives us a measure of the *hfi* constant $a_{iso} + T_{ZZ}$.

From the axial symmetry of the $[MoO(SPh)_4]^-$ complex, we can reasonably expect the *hfi* and *nqi* tensors of ^{17}O also to be axial, with the main axes being parallel to the Mo≡O bond (molecular axis *z*). Therefore, our analysis of the experimental data will be based on this approximation. At the end, however, we will return to a discussion of how good this approximation really is in quantitative terms.

If the main axes of the axial *g*- and *hfi* tensors are collinear, then the anisotropic *hfi* constant at a given EPR position is simply $T_{ZZ} = T_\perp(1 - 3\cos^2\theta)$, where θ is found from eq 11. The dependence of the splitting between the experimental ν^1_α and ν^1_β lines, $A = a_{iso} + T_{ZZ}$, on $1 - 3\cos^2\theta$ is shown in Figure 3a. As expected, this dependence is linear, and a least-squares linear fit yields the approximate *hfi* parameters $a_{iso} \approx 6.3$ MHz and $T_\perp \approx 1.6$ MHz.

These *hfi* parameters will be used as an initial approximation in numerical simulations described below. To perform these simulations, however, one also needs to obtain an initial approximation for the *nqi* parameters. From the analysis given in the Theory section, it follows that the most suitable experimental parameter that can be utilized for measuring the quadrupole coupling constant is the splitting between the component lines in the sum combination quintet $\nu^1_\sigma(m_I)$ (see eqs 6 and 7).

The primary ESEEM spectra in Figure 2 did not reveal any splittings in the ν^1_σ line, the most plausible reason being an insufficient frequency resolution of the primary ESEEM technique limited by the transverse relaxation time of the electron spin. As an alternative, one can use the four-pulse ESEEM technique that also exhibits the sum combination line.[44] In this case, however, the spectral resolution may be much higher than in the primary ESEEM spectra because it is now determined

(44) Van Doorslaer, S.; Schweiger, A. *Chem. Phys. Lett.* **1997**, *281*, 297−305.

by the electron spin longitudinal relaxation time. To our knowledge, using the four-pulse ESEEM for resolving quadrupole splittings of the ν_σ^1 line in the case of $I = 5/2$ was only discussed theoretically,[38−41] while the experimental attempts to observe these splittings were not successful. In this work, because of the well-defined structure and axial symmetry of the $[Mo^{17}O(SPh)_4]^-$ complex, we were able to resolve the *nqi* splittings of the sum combination line. These experiments are described in detail below.

Integrated Four-Pulse ESEEM Spectra. Determination of *nqi* Parameters. In this work, to increase the resolution of the sum combination line, the four-pulse ESEEM technique with integration over the time interval between the first two pulses, τ, was used. The advantage of the integrated four-pulse ESEEM technique is that all τ-dependent terms average out, and a one-dimensional (1D) spectrum with nearly zero dead time can be obtained.[45]

The integrated four-pulse ESEEM spectra of $[Mo^{17}O(SPh)_4]^-$ obtained at EPR positions A, B, and C are shown in Figure 4. In spectrum A ($\theta \approx 11°$), the generic sum combination line clearly splits into a quintet of separate lines $\nu_\sigma^1(m_I)$, with $|\Delta\nu_\sigma^1| \approx 0.4$ MHz. A quintet splitting is also observed in spectrum C ($\theta \approx 79°$), but in this case, it is about half as large, $|\Delta\nu_\sigma^1| \approx 0.2$ MHz. In spectrum B ($\theta \approx 56°$), no splitting is observed. This behavior is consistent with an axial or nearly axial *nqi* tensor, in which case the sign of $\Delta\nu_\sigma^1$ for the angles $\theta < 54.7°$ (the magic angle) is to be opposite to the sign of $\Delta\nu_\sigma^1$ for $\theta > 54.7°$. The dependence of $\Delta\nu_\sigma^1$ on $1 - 3\cos^2\theta$ obtained from the four-pulsed ESEEM measurements at EPR positions A, B, and C, as well as at several other positions, is shown in Figure 3b. The sign of $\Delta\nu_\sigma^1$ at $\theta < 54.7°$ was tentatively taken as negative. Changing this sign to the opposite will ultimately result in a change of the sign of the quadrupole coupling constant. Both assignments, however, will result in identical ESEEM spectra.

The splitting between the component lines in the $\Delta\nu_\sigma^1$ quintet is described by eq 7, where $\tilde{Q} = 3/2k[3\cos^2\theta - 1]$ for an axial *nqi* tensor ($\eta = 0$). From a linear least-squares fit to the data in Figure 3b, one can then estimate $e^2Qq/h = 40k \approx 1.48$ MHz. This quadrupole coupling constant, along with the *hfi* parameters estimated above, was used as an initial approximation in numerical simulations of the primary and integrated four-pulse ESEEM spectra.

Numerical Simulations of the ESEEM Spectra. Numerical simulations were performed using the home-written software SimBud[46] that allows one to simulate various orientation-selective pulsed EPR experiments. In the simulations, the *hfi* and *nqi* parameters determined from the plots in Figure 3 were used as an initial approximation. The simulations assuming axial *hfi* and *nqi* tensors whose main axes are parallel to the main axis of the g-tensor have resulted in $a_{iso} = 6.5 \pm 0.1$ MHz, $T_\perp = 1.6 \pm 0.1$ MHz, and $e^2Qq/h = 1.45 \pm 0.05$ MHz. One can see that the simple estimates of the *hfi* and *nqi* parameters made using the plots in Figure 3 were actually very accurate. The examples of simulated spectra are shown by dashed traces in Figures 2 and 4.

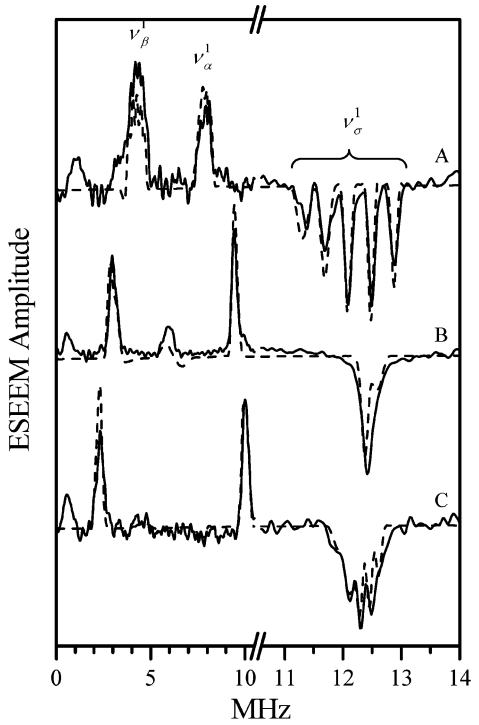

Figure 4. Solid traces A, B, and C, cosine Fourier transforms (low-frequency part) of integrated four-pulse ESEEM of $[Mo^{17}O(SPh)_4]^-$ obtained at EPR positions A, B, and C, respectively (see Figure 1). Experimental conditions: mw frequency = 29.372 GHz; mw pulses = 14, 14, 17, and 14 ns; dead time = τ_d = 20 ns. Dashed traces are the corresponding simulated spectra of the integrated four-pulse ESEEM. The simulation parameters are the same as in Figure 2. The assignments of the clearly visible lines are indicated.

The percentage of ^{17}O-substituted $[MoO(SPh)_4]^-$ was estimated as the ratio of the experimental and calculated primary ESEEM amplitudes. The resulting ^{17}O enrichment was only about 28%, which was unexpectedly low, given the 70% ^{17}O enrichment of H_2O used to synthesize the complex. This fact, however, is in line with an earlier observation[6] of disappearance of the $[Mo^{17}O(SPh)_4]^-$ EPR signal in about 20 min after dissolving the solid compound in CH_3CN, when the experiment was performed in a liquid phase. This disappearance was explained by exchange of the oxo-^{17}O with residual water in the solvent.

Finally, we have used the numerical simulations to investigate possible departures of the *hfi* and *nqi* parameters from the ideal axial model employed above. Such departures may be caused by small distortions of the complex geometry that usually take place in a frozen solution. The results of these extended simulations are summarized as follows: the minimal ratio of the two small components of the *hfi* tensor, $T_{22}/T_{11} \geq 0.7$ ($T_{22}/T_{11} = 1$ corresponds to the axial tensor), the angle between the main *hfi* axis, and the main axis of the g-tensor, $\theta_h \leq 5°$; the *nqi* asymmetry parameter, $\eta \leq 0.15$; the angle between the main *nqi* axis and the main axis of the g-tensor, $\theta_q \leq 10°$. One can see from these results that the possible departures from axiality are actually very small, and the C_4 symmetry of $[MoO(SPh)_4]^-$ in frozen solution is preserved with good accuracy.

Qualitative Discussion of the *nqi* and *hfi* Parameters. To discuss the ^{17}O *nqi* and *hfi* data in terms of electronic and spin populations of the oxygen orbitals, we have to specify the orbital model appropriate for the description of the Mo≡O group. Three

(45) Astashkin, A. V.; Raitsimring, A. M. *J. Magn. Reson.* **2000**, *143*, 280−291.
(46) Astashkin, A. V.; Raitsimring, A. M. Available for download from *http://quiz2.chem.arizona.edu/epr*, 2005.

out of four valence orbitals of the oxygen atom (or rather O^{2-} ion) participate in the Mo≡O bond. One of these orbitals represents a general hybrid of p_z and s orbitals and makes a σ-bond with the d_{z^2} orbital of Mo(V). The s-character of this orbital, χ_{s1}, is difficult to predict from qualitative considerations, and the values from $\chi_{s1} = 0$ (pure p_z orbital) to $\chi_{s1} = 1/2$ (conventional sp hybrid) are conceivable. Despite this uncertainty, we will still denote this orbital as sp_{z1}.

Two more oxygen orbitals participating in the Mo≡O bond are the p_x and p_y orbitals that make π-bonds with, respectively, d_{xz} and d_{yz} orbitals of molybdenum. The fact that these orbitals are virtually pure p-orbitals follows from the C_4 symmetry of the complex and from the axial symmetry of the g-tensor and the *hfi* and *nqi* tensors of ^{17}O.

The fourth valence orbital of oxygen does not participate in the bonding with molybdenum. This orbital, sp_{z^2}, like the bonding orbital sp_{z^1} discussed above, is also a general sp hybrid. The s-character of sp_{z^2}, $\chi_{s^2} = 1 - \chi_{s^1}$, can assume the values from 1/2 to 1.

Let us consider first the ^{17}O quadrupole interaction tensor. The axial *nqi* tensor that corresponds to the quadrupole coupling constant $e^2Qq/h \approx \pm 1.45$ MHz can explicitly be written as $(P_{xx},P_{yy},P_{zz}) \approx \pm(-0.036,-0.036,0.072)$ MHz.[47] The *nqi* tensor associated with a single electron in a p-orbital is approximately $(-0.52,-0.52,1.04)$ MHz ($e^2Qq/h \approx 20.8$ MHz[48]). If all of the oxygen valence orbitals are fully occupied, then the total *nqi* coupling constant would be zero. A nonzero *nqi* coupling constant appears because the bonding sp_z orbital and the p_x and p_y orbitals donate part of their electronic populations to d_{z^2}, d_{xz}, and d_{yz} orbitals of Mo(V). The z-component of the *nqi* tensor can be expressed as

$$P_{zz} = 2P_{||}^{p}(1 - \chi_{s^2}) + (2 - \delta_{sp_{z1}})P_{||}^{p}(1 - \chi_{s_1}) - (2 - \delta_{p_x})\frac{P_{||}^{p}}{2} - (2 - \delta_{p_y})\frac{P_{||}^{p}}{2} \quad (13)$$

where $P_{||}^{p} = 1.04$ MHz is the parallel component of the *nqi* tensor associated with a single electron on a p-orbital of ^{17}O. The first term describes the contribution of the sp orbital of oxygen that does not participate in bonding with molybdenum (sp_{z^2}), while the other three terms are the contributions of the bonding orbitals. The factors in front of each $P_{||}^{p}$ and $P_{||}^{p}/2$ are the electronic populations of the oxygen orbitals, and δ_{p_x}, δ_{p_y}, and $\delta_{sp_{z1}}$ are the parts of these populations donated to molybdenum.

Substituting $P_{zz} = \pm 0.072$ MHz into eq 13 and taking into account that $\chi_{s^2} = 1 - \chi_{s^1}$ and $\delta_{p_x} = \delta_{p_y}$ (because of the axial symmetry of the experimental *nqi* tensor), we can easily estimate $\delta_{p_x} = \delta_{p_y} \approx (1 - \chi_{s^1})\delta_{sp_{z1}} \pm 0.07$. Since the typical values of δ are expected to be considerably greater than 0.07, it appears that it is a relatively minor imbalance in the population transfer from different orbitals that results in the observed ^{17}O *nqi* coupling. Neglecting this imbalance results in $\delta_{p_x} = \delta_{p_y} \approx (1 - \chi_{s^1})\delta_{sp_{z1}}$. In the limiting case of $\chi_{s^1} = 1/2$ (a conventional sp_z orbital), one obtains $\delta_{p_x} = \delta_{p_y} \approx \delta_{sp_{z1}}/2$, which may be interpreted as an indication that the π-bonds are twice as weak as the σ-bond. The other limiting case of $\chi_{s^1} = 0$ (pure p_z orbital), one obtains $\delta_{p_x} = \delta_{p_y} \approx \delta_{sp_{z1}}$, indicating that all the π- and σ-bonds are of the same strength.

While the analysis of the *nqi* gives information about the electronic populations of the oxygen orbitals, the analysis of the *hfi* provides one with spin populations of these orbitals. Although the unpaired electron mainly occupies the d_{xy} orbital, other orbitals of molybdenum, including those participating in the bond formation with the axial oxygen, acquire some spin population via a polarization mechanism. This spin population is further propagated to the oxygen orbitals and determines or, at least, affects the *hfi* of the oxo-^{17}O. The *hfi* parameters can be qualitatively analyzed using the following equations that relate the observed isotropic and anisotropic *hfi* parameters of ^{17}O with the spin populations of its bonding orbitals:

$$T_{xx} = \frac{g\beta g_n\beta_n}{hR_{MoO}^3}\rho_{Mo} + b_p(1 - \chi_{s1})\rho_{sp_{z1}} - 2b_p\rho_{p_x} + b_p\rho_{p_y}$$

$$T_{yy} = \frac{g\beta g_n\beta_n}{hR_{MoO}^3}\rho_{Mo} + b_p(1 - \chi_{s1})\rho_{sp_{z1}} + b_p\rho_{p_x} - 2b_p\rho_{p_y}$$

$$a_{iso} = (a_s\chi_{s1} + a_p(1 - \chi_{s1}))\rho_{sp_{z1}} + a_p(\rho_{p_x} + \rho_{p_y}) \quad (14)$$

where g and g_n are the electronic and nuclear g-factors, respectively, β is the Bohr magneton, β_n is the nuclear magneton, and h is Planck's constant. The characteristic isotropic *hfi* constants $a_s \approx -5260$ MHz and $a_p \approx -120$ MHz, and the anisotropic *hfi* constant $b_p \approx 170$ MHz correspond to a spin population of $\rho = 1$ localized in a s or p (as indicated by a subscript) orbital of oxygen.[49,50] The spin population on Mo, ρ_{Mo}, and the molybdenum−oxygen distance, R_{MoO}, represent variable parameters that are known with a certain degree of accuracy, while the spin populations on various oxygen orbitals, $\rho_{sp_{z1}}$, ρ_{p_x}, and ρ_{p_y} are the values we want to estimate. Since the anisotropic *hfi* is axial ($T_{xx} = T_{yy} \equiv T_\perp$), the spin populations ρ_{p_x} and ρ_{p_y} should be similar, and we will simply set $\rho_{p_x} = \rho_{p_y}$.

In our experiments, we have determined that a_{iso} and $T_\perp$ have the same signs. The absolute signs are, however, unknown. Therefore, we have to consider the solutions for two possible sets of *hfi* parameters: (1) $a_{iso} = 6.5$ MHz, $T_\perp = 1.6$ MHz, and (2) $a_{iso} = -6.5$ MHz, $T_\perp = -1.6$ MHz. To solve eqs 14 with respect to oxygen spin populations, we will assume $\rho_{Mo} \sim 0.8$ and take $R_{MoO} = 1.7$ Å.[6] Substituting all the necessary parameters into eqs 14, we can now easily estimate the values of ρ_{p_x}, ρ_{p_y}, and $\rho_{sp_{z1}}$ as a function of s-character of the σ-bonding orbital, χ_{s^1}. The estimates for the two limiting cases of $\chi_{s^1} = 0$ (σ-bonding orbital is pure p_z) and $\chi_{s^1} = 1/2$ (σ-bonding orbital is a conventional sp_z hybrid) are presented in Table 1.

It seems that at least some of the spin populations estimated for $\chi_{s^1} = 1/2$ are about an order of magnitude too small, while those estimated for $\chi_{s^1} = 0$ seem to be reasonable. Although this may be taken as an indication that the σ-bonding orbital is closer to a pure p-orbital than to the conventional sp hybrid, this is really not a solid ground to prefer one hybridization over the other. Also the analysis of the ^{17}O *nqi* performed above gives reasonable electronic populations for both kinds of

(47) The *nqi* tensor principal components are: $P_x = -k(1 - \eta)$, $P_y = -k(1 + \eta)$, and $P_x = 2k$, where $k = e^2Qq/[4I(2I - 1)h]$ and η is the asymmetry parameter of the electric field gradient on the nucleus.

(48) Kamper, R. A.; Lea, K. R.; Lustig, C. D. *Proc. Phys. Soc., London* **1957**, *70B*, 897−899.

(49) Morton, J. R.; Preston, K. F. *J. Magn. Reson.* **1978**, *30*, 577−582.

(50) Zhidomirov, G. M.; Schastnev, P. V.; Chuvylkin, N. D. *Quant. Chem. Calc. Magn. Reson. Param.: Free Radicals* **1978**, 367.

Table 1. Spin Populations in the Bonding Oxygen Orbitals Estimated Using Equation 14 for the Limiting Cases of $\chi_{s^1} = 0$ (σ-bonding orbital is pure p_z) and $\chi_{s^1} = 1/2$ (σ-bonding orbital is a conventional sp_z hybrid) and the Different Possible Signs of the *hfi* Parameters.

	$a_{iso} = 6.5$ MHz $T_\perp = 1.6$ MHz $\chi_{s^1} = 0$	$a_{iso} = -6.5$ MHz $T_\perp = 1.6$ MHz $\chi_{s^1} = 0$	$a_{iso} = 6.5$ MHz $T_\perp = -1.6$ MHz $\chi_{s^1} = 1/2$	$a_{iso} = -6.5$ MHz $T_\perp = -1.6$ MHz $\chi_{s^1} = 1/2$	B3LYP[a]
ρ_{p_x}, ρ_{p_y}	−0.018	0.025	−0.0004	0.02	−0.017[b]
$\rho_{sp_{z1}}$	−0.019	0.005	−0.0024	0.0006	−0.017

[a] Calculated according to the Löwdin partitioning scheme from calculations on the X-ray structure. [b] Averaged to axial symmetry. The anisotropy is 0.003 unpaired electrons.

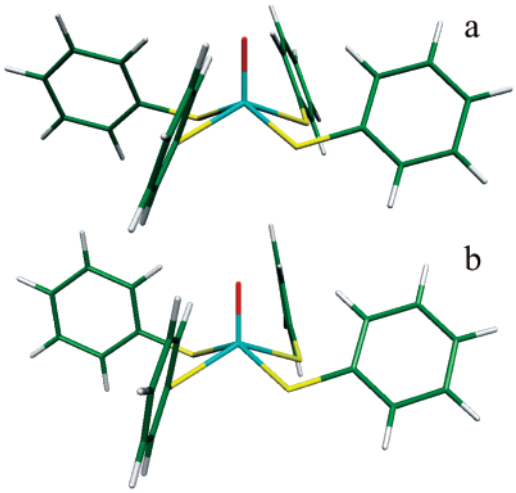

Figure 5. Comparison of the optimized (a) and experimental (b) structures of $[MoO(SPh)_4]^-$.

hybridization. Therefore, in the following section, we will compare our spin and electronic population estimates with the results of quantum-chemical (DFT) calculations.

Results of DFT Calculations. The purpose of the DFT calculations was to provide an understanding of the electronic structure of $[Mo^{17}O(SPh)_4]^-$ that leads to the observed *hfi* and *nqi* parameters of the ^{17}O-oxo ligand. We were particularly interested in answers to the questions that created uncertainties in our qualitative analysis performed above. Namely, what is a hybridization of the oxygen valence orbitals, and what are the absolute signs of the *hfi* parameters? However, while our qualitative analysis was performed for an isolated subset of the orbitals, DFT calculations involve all of the electrons in the complex anion. Therefore, before discussing the magnetic resonance parameters of the ^{17}O ligand, one has to evaluate the overall quality of the DFT calculations.

The experimental[4] and BP86/ZORA optimized structures are shown in Figure 5. The Mo−O bond is predicted slightly too long (by ∼0.05 Å, similar to what has been found in a related study[51]). Likewise, the Mo−S bonds are computed slightly too long (by ∼0.03−0.05 Å), but the overall agreement is reasonable, and the ligand positions and ring orientations are largely preserved in the computed structure.

The overall electronic structure of the complex has been analyzed in detail before[52,53] and needs little additional explanation. The singly occupied MO is of the weakly π-antibonding type (Mo $4d_{xy}$ based) and oriented perpendicular to the Mo≡O

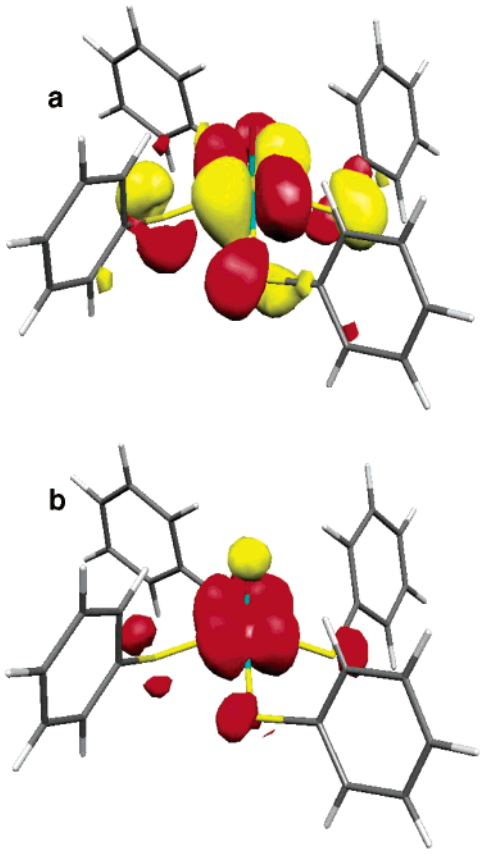

Figure 6. (a) The singly occupied spin unrestricted natural orbital of $[MoO(SPh)_4]^-$ contoured at 0.05 $(e/bohr^3)^{1/2}$. (b) The total spin density of $[MoO(SPh)_4]^-$ contoured at 0.001 $e/bohr^3$. The calculations used the experimental geometry and the scalar relativistic B3LYP/ZORA functional together with large, uncontracted Gaussian basis sets.

triple bond which dominates the ligand field (Figure 6). The net spin density roughly follows the shape of the singly occupied molecular orbital (SOMO) with one important exception; due to spin-polarization, a significant amount (−0.063 electrons in the Mulliken analysis and −0.048 electrons in the Löwdin analysis) of negative spin population appears on the oxo-oxygen. According to either the Löwdin or the Mulliken analysis, 80−82% of the positive spin population is located in the Mo 4d-orbitals, and 3−4% of the spin population resides on each of the sulfur atoms. Spin populations on carbons and hydrogens are fairly small.

The calculated EPR parameters show encouraging agreement with the experimental values (see Table 2). The effects of the solvent correction are very limited (as found in a related study[51]) and are, therefore, not further documented. The effects of the scalar relativistic correction at the ZORA level are somewhat larger and improve the agreement with the experimental values for all quantities. The ZORA effect on the g-tensor is reasonably

(51) Cosper, M. M.; Neese, F.; Astashkin, A. V.; Carducci, M. D.; Raitsimring, A. M.; Enemark, J. H. *Inorg. Chem.* **2005**, *44*, 1290−1301.
(52) McMaster, J.; Carducci, M. D.; Yang, Y.; Solomon, E. I.; Enemark, J. H. *Inorg. Chem.* **2001**, *40*, 687−702.
(53) McNaughton, R. L.; Tipton, A. A.; Rubie, N. D.; Conry, R. R.; Kirk, M. L. *Inorg. Chem.* **2000**, *39*, 5697−5706.

Table 2. Comparison of Experimental Magnetic Resonance Parameters of $[Mo^{17}O(SPh)_4]^-$ with Those Calculated by DFT

	Experimental	Experimental Structure		Optimized Structure	
		BP86	B3LYP	BP86	B3LYP
g_1	1.982	1.9889	1.9831	1.9908	1.9839
g_2	1.982	1.9900	1.9844	1.9918	1.9850
g_3	2.020	2.0275	2.0251	2.0247	2.0224
$A_1(^{95}Mo)$ (MHz)	66	31.75	49.23	30.25	47.85
$A_2(^{95}Mo)$ (MHz)	66	31.92	49.43	30.49	48.10
$A_3(^{95}Mo)$ (MHz)	157	111.94	144.68	107.54	141.51
a_{iso} (^{17}O) (MHz)	6.5 ± 0.1	2.00	4.39	2.93	4.16
$T_\perp$ (^{17}O) (MHz)	1.6 ± 0.1	1.96	2.24	0.57	2.47
e^2qQ/h (MHz)	1.45 ± 0.05	1.069	1.024	0.790	0.737
η	≤ 0.15	0.25	0.2	0.13	0.15

small (∼2−4 ppt). The Mo *hfi*'s are smaller by ∼10 MHz if the ZORA correction is not applied, while the oxygen *hfi*'s are affected by less than 0.1 MHz. The ^{17}O *nqi* calculated in the nonrelativistic limit is 12% smaller than the ZORA value.

The predicted g-tensor correctly reproduces the experimental finding that one principal g-value is larger than the free electron g-value, while the two perpendicular components are below it. This is unusual for a d^1 system, where all ligand field excited states only contribute to negative shifts. To understand this finding, one has to go beyond ligand field theory and take into account ligand-to-metal charge transfer excitations, which are particularly low-lying in the thiolate-ligated Mo(V) complexes. The anisotropy in the ^{95}Mo *hfi* is predicted with excellent accuracy. The Fermi contact term is, however, underestimated by 20% (for the B3LYP functional) or more (for the pure GGA functional BP86) owing to insufficient core level spin-polarization.[34,54,55]

The calculated isotropic component of the ^{17}O *hfi* is positive and ∼2 MHz smaller than the experimental estimate of 6.5 MHz. The SOC correction is quite small and amounts to 0.1−0.3 MHz on the individual tensor components. The calculated anisotropy in the *hfi* thus mainly stems from the spin-dipolar part and appears to be slightly overestimated by the calculations. The agreement is nevertheless fairly reasonable, especially given that all contributions to the *hfi* are indirect, through spin-polarization and through-space interactions.

The calculated *nqi* tensor also reasonably compares with the experimental estimate. Better agreement (1.05 MHz for e^2qQ/h calculated vs 1.45 MHz measured experimentally) is found for the calculations based on the experimental structure, which shows somewhat less symmetry than the optimized structure. The calculated value, although off by ∼50%, is still quite good considering how small the quadrupole coupling constant is (recall that a single electron in an oxygen p-orbital gives e^2qQ/h ∼15−20 times larger than the observed and calculated values).

Since the overall agreement between calculation and experiment is reasonable, it is possible to use the calculation results to evaluate the qualitative model from the previous section. In doing so, it should be stressed that individual atomic or orbital spin and charge populations are not observables in the strict quantum mechanical sense. They are nevertheless good guides in approaching a qualitative understanding of the experimental spectroscopic parameters. Below, we compare Löwdin spin populations from the B3LYP calculations on the experimental structure with the experimental estimates.

Turning first to the spin populations in the oxygen valence orbitals, the Löwdin analysis predicts a negative spin population of −0.017 electrons in the oxygen p_σ orbital, while the total π-spin population amounts to −0.035, which shows that all three oxygen p-orbitals carry about the same spin population. The spin population in the oxygen 2s orbital is quite small and amounts to −0.0004 electrons, which is 2 orders of magnitude smaller than the p-spin population. Thus, from this point of view, there is very little evidence for significant sp^n hybridization at the oxo group. The equivalence of the π- and σ-bonds is also shown by approximate equality of the electronic populations of oxygen p-orbitals (∼1.54 electrons/orbital).

From the analysis presented above, the calculations definitely favor the solution which has $\chi_{s^1} = 0$ with both a_{iso} and $T_\perp$ positive. The first column in Table 1 shows the oxygen spin populations estimated from eq 14 for $\chi_{s^1} = 0$ and positive a_{iso} and $T_\perp$. One can see that they are in excellent agreement with those predicted by DFT (last column in Table 1). Also, the qualitative consideration of the *nqi* for $\chi_{s^1} = 0$ (eq 13) resulted in the electronic populations of oxygen bonding orbitals being approximately equal, in agreement with the DFT results (although, unlike DFT, it only shows the differences in the electronic populations). The significance of this result is in the easy applicability of the local qualitative treatment to more complicated systems, where the structural information about the complex may be limited, and the conditions for rigorous quantum-chemical calculations are not well defined.

Conclusions

In this work, we used K_a band ESEEM spectroscopy to determine the *hfi* and *nqi* parameters for the ^{17}O nucleus of an axial oxo ligand in $[Mo^{17}O(SPh)_4]^-$, a model for the *axial* oxo ligand of the molybdenum center of sulfite oxidase. The isotropic *hfi* constant found for the oxo-^{17}O, $a_{iso}(^{17}O) = 6.5$ MHz, is very small compared to the values of ∼20−40 MHz typical for the ^{17}O nucleus of *equatorial* $OH_{(2)}$ ligand in molybdenum enzymes.[11,13,56−58] The ^{17}O *nqi* parameters presented here are, to our knowledge, the first determination of the *nqi* parameters for an oxo group in a metal complex. The quadrupole coupling constant ($e^2qQ/h = 1.45$ MHz) for the oxo-^{17}O ligand in a molybdenum complex is substantially smaller than the ∼6.5 MHz found for $^{17}OH_2$ ligands in other metal complexes.[59,60]

(54) Munzarova, M. L.; Kubacek, P.; Kaupp, M. *J. Am. Chem. Soc.* **2000**, *122*, 11900−11913.
(55) Munzarova, M.; Kaupp, M. *J. Phys. Chem. A* **1999**, *103*, 9966−9983.
(56) Gutteridge, S.; Malthouse, P. G.; Bray, R. C. *J. Inorg. Biochem.* **1979**, *11*, 355−360.
(57) Bray, R. C.; Gutteridge, S. *Biochemistry* **1982**, *21*, 5992−5999.
(58) Xia, M.; Dempski, R.; Hille, R. *J. Biol. Chem.* **1999**, *274*, 3323−3330.

The EPR parameters of $[Mo^{17}O(SPh)_4]^-$ predicted by relativistic DFT calculations are in very good agreement with those obtained by experiment. Particularly encouraging is the close similarity between the calculated and observed *hfi* and *nqi* parameters of the oxo-^{17}O ligand, considering how small these interactions are in the present case. The calculations also clearly show that the SOMO alone does not accurately represent the spin density in the molecule. For $[Mo^{17}O(SPh)_4]^-$, the SOMO is almost entirely molybdenum d_{xy} and sulfur p, with essentially no oxygen character. However, spin polarization mechanisms lead to significant negative spin density on the oxo group.

The close agreement between experimental and calculated EPR parameters for this high-symmetry model system provides encouragement to extend the theoretical calculations of spectral parameters to enzyme sites of lower symmetry. On the other hand, these calculations eliminate uncertainties about the hybridization of the oxygen orbitals and the sign of the spin density delocalized on this oxygen, and allow one to more productively use the qualitative approach for the interpretation of the *hfi* and *nqi* parameters in terms of spin and electronic populations.

Finally, it appears that the *hfi* and *nqi* parameters determined and analyzed in this work for an axial ^{17}O ligand are sufficiently characteristic to enable direct experimental identification of the oxo ligand in a variety of chemical and biological systems. In particular, our results strongly support the earlier hypothesis[12] that the weakly magnetically coupled ($a_{iso} \sim 5$ MHz) ^{17}O nucleus observed in the high-pH (*hpH*) form of chicken liver sulfite oxidase arises from an axial oxo ligand.

Acknowledgment. We thank Anthony G. Wedd for helpful discussions. We gratefully acknowledge support by the National Institutes of Health (GM-37773 to J.H.E.) and grants from the National Science Foundation (DBI-0139459, DBI-9604939, and BIR-9224431) for construction of the pulsed EPR spectrometers. E.B. acknowledges support as a Beckman Scholar through a grant to the University of Arizona from the Beckman Foundation. F.N. acknowledges financial support within the priority program 1137 of the German Science Foundation as well as from the German−Israeli Foundation.

Supporting Information Available: Cosine Fourier transforms of the primary ESEEM of $[Mo^{17}O(SPh)_4]^-$ obtained at EPR positions A and C, and the corresponding spectra for $[Mo^{16}O(SPh)_4]^-$ (Figure S1). Geometry optimized coordinates of $[MoO(SPh)_4]^-$ (Table S1). The material is available free of charge via the Internet at http://pubs.acs.org.

JA055472Y

(59) Raitsimring, A. M.; Astashkin, A. V.; Baute, D.; Goldfarb, D.; Caravan, P. *J. Phys. Chem. A* **2004**, *108*, 7318−7323.
(60) Thomann, H.; Bernardo, M.; Goldfarb, D.; Kroneck, P. M. H.; Ullrich, V. *J. Am. Chem. Soc.* **1995**, *117*, 8243−8251.